European Journal of Pharmaceutics and Biopharmaceutics 74 (2010) 483–494

Contents lists available at ScienceDirect

European Journal of Pharmaceutics and Biopharmaceutics

journal homepage: www.elsevier.com/locate/ejpb

Research paper

Cytotoxicity study of ordered mesoporous silica MCM-41 and SBA-15 microparticles on Caco-2 cells

Teemu Heikkilä [a,e,*], Hélder A. Santos [b], Narendra Kumar [c], Dmitry Yu. Murzin [c], Jarno Salonen [a], Timo Laaksonen [b], Leena Peltonen [b], Jouni Hirvonen [b], Vesa-Pekka Lehto [a,d]

[a] Department of Physics and Astronomy, University of Turku, Turku, Finland
[b] Division of Pharmaceutical Technology, University of Helsinki, Helsinki, Finland
[c] Process Chemistry Centre, Åbo Akademi University, Turku, Finland
[d] Department of Physics, University of Kuopio, Kuopio, Finland
[e] Graduate School of Materials Research (GSMR), Turku, Finland

ARTICLE INFO

Article history:
Received 4 December 2008
4 November 2009
Accepted in revised form 10 December 2009
Available online 16 December 2009

Keywords:
Mesoporous silica
Microparticle
Cytotoxicity
Cell viability
Biocompatibility
Caco-2
Oral drug delivery

ABSTRACT

Cytotoxicity of ordered mesoporous silica MCM-41 and SBA-15 microparticles (fractions between 1 and 160 μm) was determined in vitro on undifferentiated human colon carcinoma (Caco-2) cell line, considering the feasibility of using these silica-based materials in oral drug formulations. The cellular endpoints employed for assessing the effects of the MCM-41 and SBA-15 microparticles on Caco-2 were: (1) cell membrane integrity by monitoring live-cell protease activity (AFC) and by employing the flow cytometry method; (2) metabolic activity by monitoring total ATP content via luminescence assay; (3) activity of apoptotic effectors by caspase-3/7 activity assay. The generation of reactive oxygen species (ROS) was also followed, specifically the hydrogen peroxide (H_2O_2) and the superoxide radical (O_2^-). MCM-41 and SBA-15 microparticles caused cytotoxic effects on the Caco-2 cells, at most tested concentrations (0.2–14 mg/ml) and incubation times (3 and 24 h). The effects on the cells included weakened cell membrane integrity, diminished cell metabolism and increased apoptotic signalling. The root cause for the cytotoxicity was heightened production of reactive oxygen species (ROS), especially the formation of the superoxide radical O_2^- already after 3 h incubation with threshold dose 1 mg/ml, apparently overwhelming the antioxidant defences and causing mitochondrial dysfunction, hence increasing the apoptotic signalling.

1. Introduction

Advancements in the use of ionic and non-ionic surfactants as structure directing agents led to the discovery of ordered mesoporous silica materials MCM-41 and SBA-15 [1–4]. These novel silica-composed (SiO_2) materials possess ordered cylindrical pore structures with tuneable pore diameters in the mesoscale (2–50 nm), providing very large internal surface areas and pore volumes. The homogenous, unidirectional nanopore systems allow efficient adsorption of wide range of molecules, making these materials highly useful in many types of applications, from separation and catalysis to medicine. Biomedical applications of ordered mesoporous silica materials have been actively studied for the past 10 years, in areas such as drug delivery and tissue engineering [5–10].

Despite the considerable interest on the biorelated applications of the ordered mesoporous silicas, relatively few studies have been published on their toxicological behaviour. The hazard of crystalline silica inhalation is well known and associated with several pulmonary pathologies. Numerous studies have evidenced that there are major differences in the pathogenic potential of different types of silica particulates, due to the high variability in their physicochemical properties [11]. Silica particles may elicit different biological responses due to crystallinity, morphology (size/shape), aggregation, surface charges, hydrophilicity, biopersistence and dose [11–17]. Still, the exact mechanism of how silica particles induce toxicity on the cellular level is not known, although several biological rationales have been suggested [18–20]. Current research points to a silica and cell surface-mediated phenomena, such as silica surface (and/or cell) production of reactive oxygen species (ROS) and silica binding to surface receptors of macrophage cells.

The properties of engineered silica nanomaterials (such as MCM-41 and SBA-15) can differ substantially from the traditional forms of silica, for example considering the surface area, which further complicates their interactions with biological systems. The biological effects of sub-micrometer size MCM-41 type ordered mesoporous silica nanoparticles (MSN's) have been studied due to their potential applications in stem-cell tracking and intra-cellular drug delivery

* Corresponding author. Laboratory of Industrial Physics, Department of Physics and Astronomy, University of Turku, FI-20014, Finland. Tel.: +358 23335653; fax: +358 23335070.
E-mail addresses: teemu.heikkila@utu.fi, teanhe@utu.fi (T. Heikkilä).

0939-6411/$ - see front matter © 2009 Elsevier B.V. All rights reserved.
doi:10.1016/j.ejpb.2009.12.006

[15,21–26]. The cytotoxic effects of MSN's (particle sizes ~100–300 nm) were found low on rat pleural mesothelial, 3T3-L1 and human mesenchymal stem cells when incubated for 1–2 h at particle concentrations of 0.10–0.25 mg/ml. However, in a recent study the systemic toxicity of sub-micrometer size MCM-41 (particle size ~150 nm) and SBA-15 (particle size ~800 nm) was deemed severe [27]. Intra-peritoneal (dose/weight 1.2 g/kg of MCM-41 or SBA-15) and intra-venous injections (dose/weight 0.24 g/kg of MCM-41) of the particles in mice resulted in death or euthanasia. The non-lethal dose limit in the intra-peritoneal site of mice was determined as 0.04 g/kg. Recently, MCM-41 and SBA-15 materials have been studied as functional excipients for oral delivery of poorly water-soluble drugs [28–32]. The feasibility of SBA-15 type ordered mesoporous silica for the oral delivery of antifungal drug itraconazole has been demonstrated in vivo (rabbits and dogs) with amounts of 40–100 mg of ordered mesoporous silica (particle size 0.2–1 μm, forming ~50 μm aggregates) used in formulations [33]. No issues regarding the toxicity of the orally administered mesoporous silica was reported (dose/weight ~0.01 g/kg). Overall, the origin for the cytotoxic response of the ordered mesoporous silicas MCM-41 and SBA-15 is not well understood, although it has been established that their cytotoxicity stems from the particles themselves and not from degradation products for example [27,34]. Still, the previous results indicate that the administered dose/weight is an important factor. Also, the route of administration may have a substantial effect on the toxicological behaviour, due to the major differences between pulmonary, parenteral and enteral routes.

So far, the potential biological effects of the MCM-41 and SBA-15 materials in the gastro-intestinal tract (GIT) have not been the specific target of studies. The purpose of the present study was to obtain in vitro data on the effects of the ordered mesoporous silicas on Caco-2 cells, a widely used in vitro model of intestinal epithelial cells due to the similarities in morphology and physiology. The use of MCM-41 and SBA-15 for the delivery of drugs via the oral route would likely be based on the use of microparticular pharmaceutical compositions due to payload advantage and ease of manufacture and formulation, warranting the use of microparticles in the present cytotoxicity study. We need to consider that oral delivery of drugs may require high doses (e.g. 200 mg) of the microparticles to be administered at frequent intervals (several doses per day). In previous in vitro studies, the tested MSN concentrations on the different cell lines have been low and not comparable to the case of oral formulation and administration. Herein, we wanted to define the particle concentration thresholds that cause clear cytotoxic effects on the Caco-2 cells. Characterizing these limits allows preliminary estimation of the gastro-intestinal (GI) biocompatibility and the feasibility of tablet dosing of the silica. The cellular endpoints employed for assessing the effects of the MCM-41 and SBA-15 microparticles on Caco-2 were: (1) cell membrane integrity by monitoring live-cell protease activity and by employing the flow cytometry method; (2) metabolic activity by monitoring total ATP content via luminescence assay; (3) activity of apoptotic effectors by caspase-3/7 activity assay. The generation of specific reactive oxygen species (ROS) was also followed as a possible root cause for silica-induced cytotoxicity, specifically the hydrogen peroxide (H_2O_2) and the superoxide radical ($O_2^{\cdot-}$).

2. Materials and methods

2.1. Preparation of ordered mesoporous silica MCM-41 and SBA-15 microparticles

Synthesis of pure siliceous MCM-41 mesoporous molecular sieve material was carried out in a 300-ml autoclave using methods mentioned in references with some modifications [2,35]. The reagents used in the synthesis were fumed silica (SiO_2, 99.9%, Sigma–Aldrich, St. Louis, MO, USA), tetramethylammonium silicate ($(CH_3)_4N(OH)\cdot 2SiO_2$, 99.99%, Sigma–Aldrich), sodium silicate ($Na_2O_7Si_3\cdot SiO_2$, 27%, Sigma–Aldrich), cetyltrimethylammonium bromide (CTAB, $CH_3(CH_2)_{15}N(CH_3)_3Br$, 99%, Sigma–Aldrich) and distilled water. A gel mixture was prepared and introduced in a Teflon cup which was inserted in a 300-ml autoclave. The autoclave was kept in a large oven, and the synthesis of MCM-41 was performed at 100 °C. After the completion of synthesis, the autoclave was taken out of the oven and quenched. Mesoporous silica MCM-41 was filtered and washed with distilled water. Drying of the sample was carried out at 110 °C for 12 h and calcinated at 550 °C for 10 h.

Synthesis of pure siliceous SBA-15 was performed in a 300-ml autoclave using methods mentioned in references with some modifications [3,36]. The reagents used in the synthesis were Pluronic P123 co-block polymer (BASF, Ludwigshafen, Germany), HCl (33–40%, J.T. Baker, Phillipsburg, NJ, USA), tetraethyl orthosilicate (TEOS, $Si(OC_2H_5)_4$, 98%, Sigma–Aldrich) and distilled water. Prepared gel was introduced in a Teflon cup and inserted into 300-ml autoclave. The autoclave was then kept in a large oven heated at 100 °C. Synthesis of SBA-15 was carried out at 100 °C for 24 h. After the completion of synthesis, the mesoporous silica was filtered and washed with 1000 ml of distilled water, dried at 100 °C for 12 h and calcinated at 500 °C for 7 h.

The synthesized mesoporous silica materials MCM-41 and SBA-15 were ball milled and sieved over seven stacked test sieves (mesh sizes of 25, 32, 45, 63, 90, 100 and 125 μm, diameter 20 cm) on a sieve shaker (Fritsch GmbH, Idar-Oberstein, Germany). The <25 μm fraction from the collecting pan was rinsed with pure ethanol (99.6%, Altia Oyj, Helsinki, Finland) on a Versapor-1200 membrane disc filter (Pall Corporation, East Hills, NY, USA) with 1.2-μm pore size and dried at 65 °C for 5 h (size fraction 1–25 μm). Five of the prepared size fractions were selected as the samples for the study and designated according to the upper nominal sieve limits as MCM/25, /45, /63, /90, /125 or SBA/25, /45, /63, /90, /125.

2.2. Sample characterization

Crystallinity and structural properties of the samples were characterized with powder X-ray diffraction (XRD) using nickel-filtered Cu K_α (λ = 1.542 Å) radiation operated at 40 kV/50 mA (PANalytical, Almelo, The Netherlands). The porous properties of the microparticles were characterized with N_2 sorption measurements on a Tristar 3000 (Micromeritics, Norcross, GA, USA) instrument at −196 °C. The samples were evacuated at 250 °C for 24 h preceding the measurements using a VacPrep (Micromeritics) degasser. The surface areas and pore characteristics were determined from the adsorption branches of the isotherms according to the Brunauer–Emmett–Teller (BET), Barrett–Joyner–Halenda (BJH) and *t*-plot methods. The particle size distributions of samples were measured with a Mastersizer 2000 (Malvern, Worcestershire, UK) laser diffraction instrument equipped with a Hydro 2000G (Malvern) wet dispersion sampler. Water was used as the dispersant with the pump and stirrer speeds at 2500 rpm and 1000 rpm, respectively. Scanning electron microscopy (SEM) was done on a S200 SEM (Cambridge, UK). The samples were sputter coated with gold prior to imaging.

2.3. Cell line and culture

The in vitro cytotoxicity tests of the mesoporous silica particles were performed with human colon carcinoma (Caco-2) cells (ATTC). Caco-2 cells were cultured in 75-cm^2 culture flasks (Corning, Corning, NY, USA) using Dulbecco's modified Eagle's medium (DMEM) supplemented with 10% fetal bovine serum, 1% non-essential amino acids, 1% L-glutamine, penicillin (100 IU/ml), and streptomycin (100 μg/ml) (all from Euroclone, Siziano, Italy). The

culture was maintained at 37 °C (BB 16 gas incubator, Heraeus Instruments GmbH, Hanau, Germany) in an atmosphere of 5% CO_2 and 95% relative humidity. The growth medium was changed every other day until the time of use. Cells from passage numbers 31–40 were used in the experiments. Prior to each test, the cells were harvested using trypsin (Euroclone)–ethylenediamine tetraacetic acid (EDTA, Sigma–Aldrich)–phosphate-buffered saline (PBS) solution (0.25% trypsin–0.05 mM EDTA) and diluted at a density of 2–5 $\times$ 10^5 cells/ml according to the assay. The cell suspension was seeded into 6- or 96-well plates (Corning) at 1–2 ml/well or 100 μl/well, respectively and incubated for about 24–48 h before the tests in order to reach confluence. The protocol assays were slightly modified from the suppliers to better adapt to our present study.

2.4. Fluorescent cell viability assay (AFC)

In this test, a single-reagent-addition fluorescence assay measures the relative number of living cells in the cell population, based on one marker for cell viability (CellTiter-Fluor™ Cell Viability Assay, Promega, Madison, WI, USA). Briefly, when the fluorogenic cell-permeant peptide substrate, glycyl-phenylalanyl-amino-fluorocoumarin (GF-AFC, Promega), is cleaved by the live-cell protease activity it releases AFC. This generates a fluorescent signal proportional to the number of living cells. The live-cell protease activity marker becomes inactive upon loss of cell membrane integrity and leakage to the surrounding culture medium. After the Caco-2 cells were attached to the 96-well plates, the wells were washed with 2 $\times$ 100 μl of 10 mM HBSS buffer solution (pH 7.4). After washing, suspensions of 0.2–14 mg/ml of mesoporous silica particles were added to the 96-well plates. The cells were then incubated at 37 °C for 3 and 24 h at a stirrer speed 25 rpm. After incubation, 100 μl of the reagent assay (GF-AFC) was added to each well. The cells were further incubated for at least 45 min. Positive (9% Triton X-100 solution, Promega) and negative (HBSS buffer solution) control wells were also used for comparison. The fluorescence was measured at an excitation and emission wavelength of 400 and 505 nm, respectively, with Varioskan Flash (Thermo Fisher Scientific Inc., Waltham, MA, USA). The cell viability as a percentage of the negative control was calculated from the fluorescent values.

2.5. Luminescent cell viability assay (ATP)

In this assay, the number of viable cells in culture is quantified based on the amount of ATP produced by metabolically active cells (CellTiter-Glo® Luminescent Cell Viability Assay, Promega). Briefly, the measurement is based on the luciferase reaction, where the mono-oxygenation of luciferin is catalyzed by luciferase in the presence of Mg^{2+}, ATP, and oxygen. The amount of ATP is directly proportional to the number of living cells present in the culture. An identical procedure to the fluorescent assay was also used here. The difference was that after the 96-well plates (containing the cells and 0.2–4/14 mg/ml of the silica microparticles) were incubated at 37 °C for 3 or 24 h, the plates were equilibrated at room temperature for about 30 min. Thereafter, 100 μl of the reagent assay was added to each well. Positive (9% Triton X-100 solution) and negative (HBSS buffer solution) control wells were also used and treated similarly as described earlier. The luminescence was measured using a Wallac 1450 MicroBeta/Trilux luminescence counter (Perkin Elmer, Waltham, MA, USA). The cell viability as a percentage of the negative control was calculated from the luminescent values.

2.6. Flow cytometer cell viability analysis

The determination of the cell toxicity in the presence of the mesoporous silica microparticles by flow cytometer method was performed as follows. Caco-2 cells were seeded at 2–3 $\times$ 10^5 cells/well in 6-well plates and allowed to attach for 24–48 h. The wells were then washed with 2 $\times$ 2 ml of HBSS buffer solution, followed by the addition of suspensions of 0.2–4 mg/ml of mesoporous silica particles to the 6-well plates. The cells were then incubated for 3 or 24 h. After incubation, the wells were washed at least three times with HBSS buffer solution to remove excess of particles, and the cells were then harvested with trypsin/EDTA solution. In order to distinguish cellular debris and living cells in the flow cytometer analysis, Caco-2 cells were further stained with propidium iodide (PI, Becton Dickinson, Franklin Lakes, NJ, USA) for 15–20 min, fixed with 4% paraformaldehyde (PFA, Fluka, St. Louis, MO, USA) in PBS for 20 min, and then centrifuged. The PFA was replaced by a fresh PFA solution, centrifuged again and diluted into a suitable volume (500–700 μl, depending on the number of cells). PI fluorescence and scattering intensity distributions of the cells were obtained by LSR II flow cytometer (Becton Dickinson) with a laser excitation wavelength of 488 nm, using FACSDiva software. Exactly 10 000 events were recorded. Untreated cells were used as controls and the background, due to particles only, was excluded.

2.7. Caspase-3/7 activity assay

Caspase-3 and -7 activity was measured as a marker of apoptosis (i.e. programmed cell death cycle) using a homogenous fluorescent assay (Apo-ONE® Homogenous Caspase-3/7 Assay, Promega). Briefly, the assay detects the caspase-3/7 activity upon addition of a substrate contained peptide-rhodamine 110 in a buffer containing detergent to lyse the cells. Caspase-3/7 cleavage of the substrate removes the peptides, leaving the fluorescent rhodamine 110. An identical procedure to those described earlier was also used here. The difference was that after the 96-well plates (containing the cells and 0.2–4 mg/ml of the silica microparticles) were incubated at 37 °C for 24 h, 100 μl of Apo-ONE® Caspase-3/7 Reagent assay was added to each well. Positive (9% Triton X-100 solution) and negative (HBSS buffer solution) control wells were also used and treated similarly as described earlier. The fluorescence was measured at an excitation and emission wavelength of 499 and 521 nm, respectively, with Varioskan Flash (Thermo Fisher Scientific Inc.). The caspase-3/7 activity is expressed as a ratio between treated and untreated cells.

2.8. Detection of reactive oxygen species (ROS)

The generation of hydrogen peroxide (H_2O_2) and superoxide radicals ($O_2^{\cdot-}$) was monitored by employing 2′,7′-dichlorodihydrofluorescein diacetate (DCF-DA, Sigma–Aldrich) staining and dihydroethidium (DHE, Sigma–Aldrich) staining, respectively. DCF-DA is non-fluorescent unless oxidized by the intra-cellular ROS. Dihydroethidium is blue fluorescent in the reduced form, which upon oxidation by superoxide radical emits red fluorescence. The cells were sequentially stained first with 5 μM DHE and with 10 μM DCF-DA for 1 h at 37 °C each. Dose- and time-dependent measurements of the generation of reactive oxygen species were done by incubating the cells with 0.2–4 mg/ml of the silica microparticles for 3 and 24 h. Hydrogen peroxide-treated cells (0.25% H_2O_2) were used as positive control for DCF-DA, whereas 100 μM of diethyldithiocarbamic acid (DDC) was used as positive control for DHE staining. DDC is a strong inhibitor of superoxide dismutase activity in cells. Cells were then washed twice in HBSS buffer, and the fluorescence was measured with Varioskan Flash (Thermo Fisher Scientific Inc.) at an excitation of 498 and 610 nm for DCF-DA and DHE, respectively. The emission wavelengths were 522 and 610 nm for DCF-DA and DHE, respectively.

2.9. Statistical analysis

Results from the viability tests are expressed as mean ± SEM. Data for single comparisons were analyzed by a Student's *t* test. Multiple comparisons data were analyzed by one-way analysis ANOVA. The criterion for significance was $p \leqslant 0.05$ for all the comparisons.

3. Results

3.1. Characterization of MCM-41 and SBA-15 samples

The XRD data of the MCM-41 and SBA-15 samples (Fig. 1) were in good agreement with literature [1–4]. The patterns of MCM/25 through to MCM/125 showed well-resolved hkl(1 0 0) peaks, as well as the peaks hkl(1 1 0), hkl(2 0 0) and hkl(2 1 0), characteristic for the unidirectional hexagonal mesopore structure. No significant change in the pore repeat distance of MCM-41 was detected, calculated from the *d*-value of the hkl(1 0 0) peak [1]. The samples SBA/125 down to SBA/63 also showed well-resolved hkl(1 0 0), hkl(1 1 0), hkl(2 0 0) and hkl(2 1 0) peaks. However, in sample SBA/25 only the peak hkl(1 0 0) was well resolved, while its pore repeat had somewhat increased. This was due to its small particle size (shorter units of diffraction) in comparison with the other samples, and also partial disordering of its ordered mesopore structure. On the high angle side (insets in Fig. 1), the XRD patterns exhibited a characteristic diffuse halo arising from the amorphous composition of the silica skeletons. The XRD data was supported by N_2 sorption measurements. The nitrogen sorption isotherms were typical type IV according to the IUPAC classification, with the inflections of the capillary condensation observed (graphs not shown). All samples were clearly mesoporous according to the N_2 ad/desorption results in Table 1. Results for particle size (laser diffraction measurements) and shape (SEM imaging) are presented in Table 2. Particle size distributions for the largest and smallest nominal size fractions are presented in the insets of the example SEM images of Fig. 2. The particle size distributions of all samples were found to fan out towards the small size range, due to small particle agglomeration as evident in the SEM pictures (Fig. 2). The relative volume of small particles (<10, <5 and <2.5 μm) in each sample is given in Table 2. The amount of these small particles increased towards the smaller particle size fractions of MCM-41, whereas the SBA-15 samples had similar small particle contents. Hence, the overtly bimodal characteristic of the size distribution of sample SBA/125 (Fig. 2b), in comparison with SBA/25 (Fig. 2d), was due to its predominantly acicular particle shape and not due to higher amount of small particles. Elongated particles with high aspect ratios are known to skew laser diffraction results correspondingly [37]. Sample SBA/25 contained only sporadic acicular particles (Fig. 2d); therefore, its size distribution was similar to the sample MCM/25 (Fig. 2c) with predominantly modular type particle morphology.

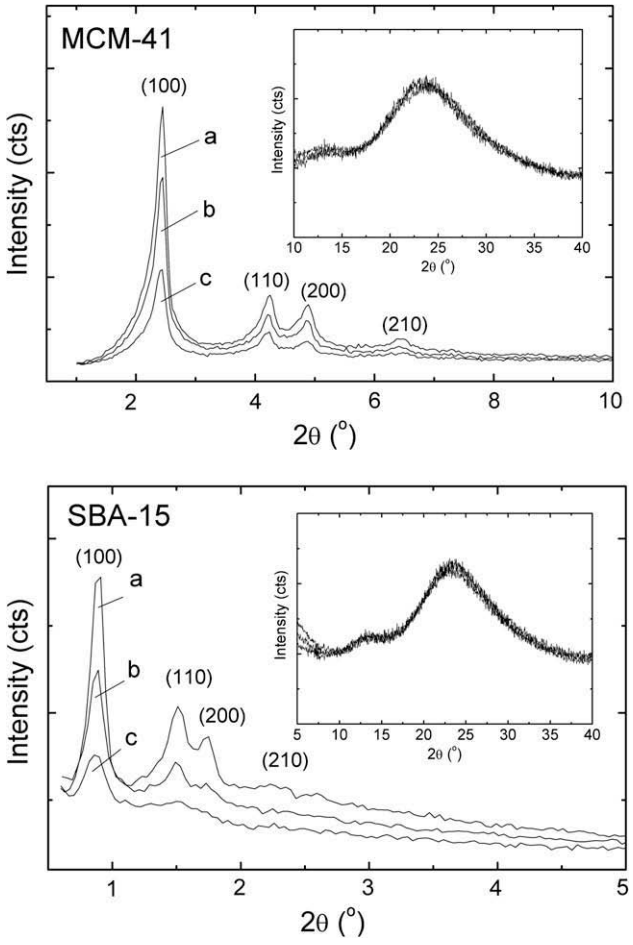

Fig. 1. XRD patterns for MCM-41 (top figure) samples: (a) MCM/125, (b) MCM/63, (c) MCM/25 and for SBA-15 (bottom figure) samples: (a) SBA/125, (b) SBA/63, (c) SBA/25.

Table 1
Textural and porous characteristics of the samples.

Sample	D_{BJH}[a] (nm)	S_{BET}[b] (m^2/g)	S_{ext}[c] (m^2/g)	V_p[d] (cm^3/g)	V_{mic}[e] (cm^3/g)	V_{mes}[f] (cm^3/g)	Porosity[g] (%)
MCM/25	3.3	731	78.8	0.612	n/a	0.407	58.3
MCM/45	3.1	688	52.0	0.520	n/a	0.389	54.3
MCM/63	3.5	909	81.5	0.785	n/a	0.551	64.2
MCM/90	3.4	918	69.5	0.767	n/a	0.550	63.7
MCM/125	3.4	935	80.6	0.789	n/a	0.576	64.3
SBA/25	4.9	534	91.8	0.651	0.034	0.484	60.1
SBA/45	4.7	476	76.7	0.549	0.045	0.421	55.9
SBA/63	5.3	535	95.6	0.709	0.040	0.514	62.1
SBA/90	5.2	534	90.2	0.682	0.056	0.516	61.2
SBA/125	5.9	597	101.8	0.880	0.051	0.678	67.1

[a] BJH average pore diameter.
[b] BET surface area.
[c] External surface area of particles (calculated by the *t*-plot method).
[d] BJH total pore volume.
[e] Micropore volume (calculated by the *t*-plot method).
[f] Mesopore volume (calculated by the *t*-plot method).
[g] Total particle porosity calculated based on the BJH total pore volume.

Table 2
Sample particle shape and size characteristics.

Sample	Particle shape[a]	D_v90[b] (μm)	D_v50[c] (μm)	<10 μm[d] (%$_{vol}$)	<5.0 μm[e] (%$_{vol}$)	<2.5 μm[f] (%$_{vol}$)
MCM/25	Modular	35.7	18.4	25.6	13.3	3.6
MCM/45	Modular	49.4	21.3	30.3	17.2	4.8
MCM/63	Modular	72.4	36.1	17.7	8.5	1.7
MCM/90	Granular	122.4	65.9	8.5	3.5	0.9
MCM/125	Granular	161.3	78.0	8.4	3.6	1.0
SBA/25	Modular	34.6	18.4	16.6	7.1	1.8
SBA/45	Modular	46.2	16.3	29.6	10.2	1.2
SBA/63	Modular	54.0	22.4	20.9	7.9	1.1
SBA/90	Granular	81.0	31.1	19.7	7.4	1.2
SBA/125	Acicular	117.4	26.9	16.3	4.2	0.2

[a] Predominant particle shape in the sample according to SEM imaging.
[b] Laser diffraction particle undersize volume 90%.
[c] Laser diffraction particle undersize volume 50%.
[d] Relative volume of particles in the sample under the size 10 μm.
[e] Relative volume of particles in the sample under the size of 5 μm.
[f] Relative volume of particles in the sample under the size of 2.5 μm.

3.2. Caco-2 cell membrane integrity (AFC and flow cytometry)

The samples MCM/25 and MCM/45 induced the earliest significant ($p \leqslant 0.05$) cell membrane integrity damage compared to control cells, already after 3 h incubation at 1 mg/ml (Fig. 3a). This was likely associated to the high relative volume of small particles in these samples, in comparison with the other samples (Table 2). The substantiated effect of MCM/25 on cell membrane integrity in comparison with sample with low relative volume of small particles, MCM/90, was also confirmed by the flow cytometry method (Fig. 4a). The effect of MCM/25 and MCM/45 was also pronounced in the 24-h test (Fig. 3b). Increasing the concentration to 4 mg/ml in the 24-h incubation test induced a significant drop in cell viability for all of the MCM-41 and SBA-15 samples, also confirmed by the flow cytometry experiment (Fig. 4b). Extensive cell damage was observed after 3 h incubation with the highest tested concentration, 14 mg/ml.

3.3. Metabolic activity of Caco-2 cells (ATP)

Significant ($p \leqslant 0.05$) decrease in the cell ATP content was observed for the majority of the samples after 3-h test at concentration of 2 mg/ml, in comparison with the control cells (Fig. 5a).

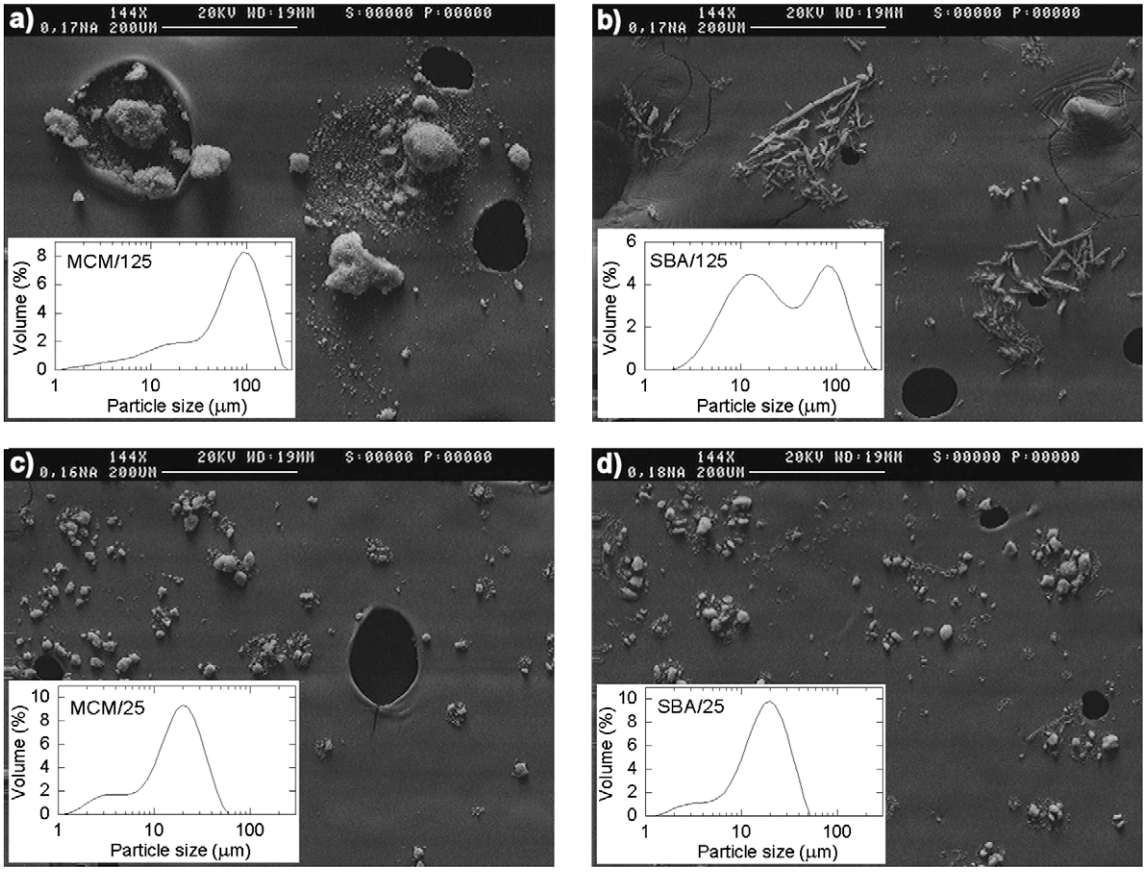

Fig. 2. Representative SEM pictures with particle size distributions of samples: (a) MCM/125, (b) SBA/125, (c) MCM/25, and (d) SBA/25. The scale in the SEM pictures corresponds to 200 μm.

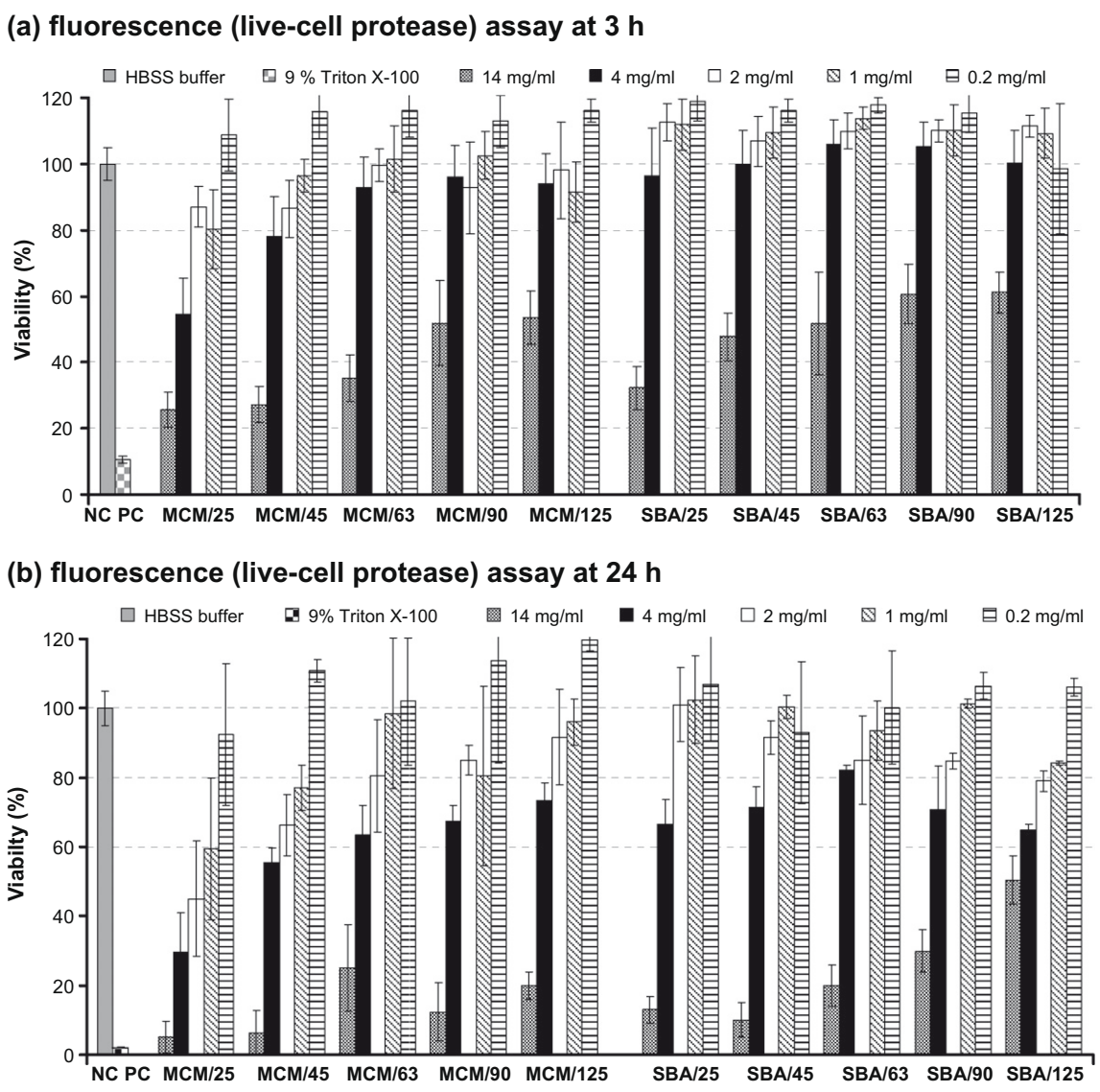

Fig. 3. Caco-2 cell viability results from fluorescence assay after: (a) 3 h and (b) 24 h incubation with MCM-41 and SBA-15 samples at 37 °C, as a function of the particle concentration and size fraction ($n \geqslant 3 \pm$ SEM).

Interestingly, there were no significant differences in the ATP content of the samples at 3 h in a head-to-head comparison of each specific concentration and particle size fraction of MCM-41 and SBA-15. At 24 h, a significant decrease in the cell ATP content was observed for the majority of the samples already at concentration of 1 mg/ml (Fig. 5b). Further effect of raising the particle concentration was not straightforward. In the majority of cases, no statistically significant differences were observed between the MCM-41 and SBA-15 materials in a head-to-head sample comparison, similar to the 3-h assay.

3.4. Caspase-3/7 activity of Caco-2 cells at 24 h

Statistically significant ($p \leqslant 0.05$) increase in the caspase-3/7 activity was detected already with the lowest tested concentration (0.2 mg/ml) of MCM/25, MCM/45 and MCM/63 (Fig. 6). However, the ~2-fold increase to control at 0.2 mg/ml was not reflected in the live-cell protease function (Fig. 3b) or cell ATP content (Fig. 5b), at least at 24 h. Overall, with MCM-41 samples the caspase-3/7 activity was increased by smaller particle size, but it was not dependent on the particle concentration beyond the threshold of 1 mg/ml. Similarly, the effect of raising the SBA-15 particle concentration above the threshold of 1 mg/ml was not statistically significant in most samples. The caspase-3/7 activity for the sample SBA/25 did not significantly differ from the sample MCM/25, indicating that the effect of the smallest particles of the different silica materials on the apoptotic signalling activity was similar. This result suggested that the substantiated effect of MCM/25 on the cell membrane integrity (Fig. 3b) in comparison with SBA/25 was not solely associated with the increased caspase-3/7 activity. Some of the high concentration SBA-15 samples (2 and 4 mg/ml) induced significantly higher caspase-3/7 activities than the corresponding MCM-41 samples (e.g. MCM/90 vs. SBA/90), which however was not reflected in the cell viability results at 24 h (Figs. 3b and 5b). The results indicated that the higher caspase-3/7 activity and related apoptosis was not the sole explanation for the reduced cell viabilities. Direct interaction between the cells and particles was another likely cytotoxic pathway involved.

3.5. Reactive oxygen species (ROS) formation

Formation of ROS in the samples, specifically hydrogen peroxide (H_2O_2) and the superoxide radical ($O_2^{\cdot-}$) species was monitored

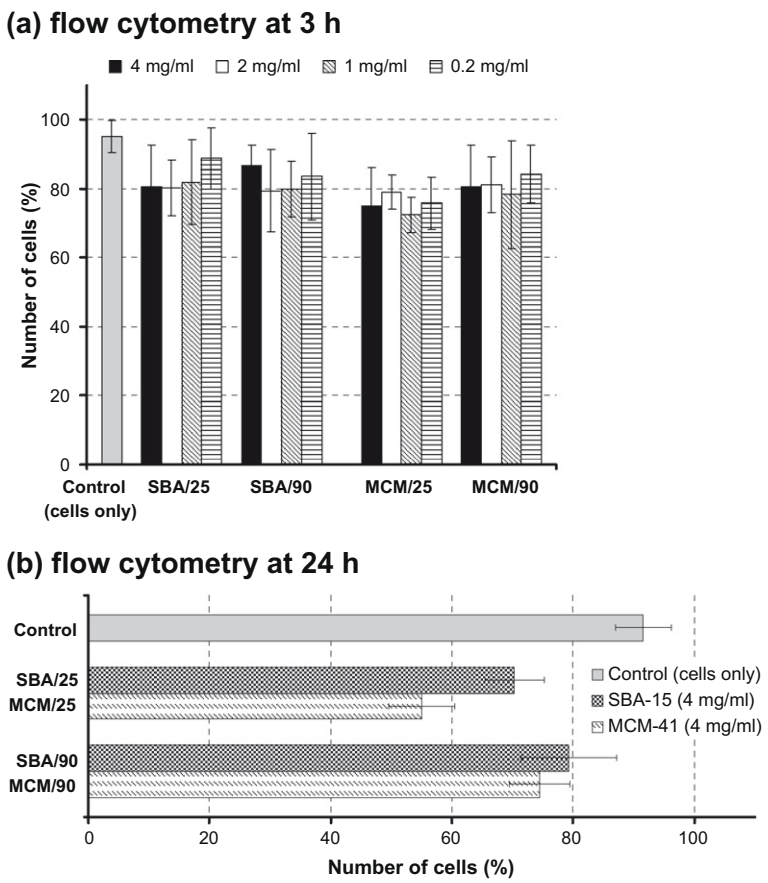

Fig. 4. Flow cytometer results for the determination of living Caco-2 cells (%) after being treated and incubated with MCM-41 and SBA-15 samples for: (a) 3 h and (b) 24 h at 37 °C, with respect to the untreated control cells ($n \geqslant 3 \pm$ SEM). MCM/25 samples were statistically different ($p \leqslant 0.05$).

(Figs. 7 and 8). No significant ($p \leqslant 0.05$) H_2O_2 formation was detected in the majority of the MCM-41 and SBA-15 samples after 3-h incubation in comparison with the control, with the systematic exception of the 1–4 mg/ml concentrations of samples MCM/25 and MCM/45 (Fig. 7a). The slight increase in H_2O_2 generation at 3 h was obviously not the sole reason for the marked reductions in the ATP assay at the same time point (Fig. 5a), for example the ATP content of sample SBA/125 had clearly decreased, while its H_2O_2 level was still well in line with the control (Fig. 7a). After 24-h incubation (Fig. 7b), the slightly lower levels of H_2O_2 formation in SBA-15 vs. MCM-41 contradicted the higher caspase-3/7 activity of SBA-15 at 24 h (Fig. 6). This suggested that the H_2O_2 formation was not solely responsible for the heightened caspase-3/7 activity in SBA-15 samples. The slight difference in the H_2O_2 forming potential of MCM-41 and SBA-15 at 24 h supported better the AFC data (Fig. 3b) than the ATP data (Fig. 5b). Still, the relationship between the H_2O_2 formation and cell viability was not obvious in many cases indicating the involvement of also other cytotoxic processes.

Significant ($p \leqslant 0.05$) increase of superoxide $O_2^{\cdot-}$ formation at 3 h was detected in most samples at 1 mg/ml, increasing to a maximum of ~2-fold to control at 4 mg/ml (Fig. 8a). The superoxide production at 3 h was not dependent on the tested particle size fraction of MCM-41 or SBA-15, thus it was better in line with the ATP assay data (Fig. 5a) than the AFC assay (Fig. 3a) at 3 h. After 24-h incubation, all samples showed a significant increase in superoxide content at concentration 1 mg/ml (Fig. 8b). Further raise of the concentration to $\geqslant$2 mg/ml increased the $O_2^{\cdot-}$ radical formation of MCM-41 samples in a concentration-dependent manner. The superoxide formation in MCM-41 at 24 h could not be directly linked to its caspase-3/7 activity at 24 h (Fig. 6), considering the drastic activity of MCM/25 in comparison with the other samples. Considering the lack of particle size dependence in the MCM-41 superoxide formation at 24 h, it was better associated with the ATP data (Fig. 5b) than the AFC data (Fig. 3b). Still, for example the similar $O_2^{\cdot-}$ formation at 4 mg/ml across the particle size ranges (Fig. 8b) did not directly support the lower ATP values obtained for MCM/25, MCM/45 and MCM/63 at 4 mg/ml (Fig. 4b), suggesting that also other cytotoxic processes were involved. In the case of SBA-15, the superoxide formation was not dependent on the tested particle size, and the effect of increasing the particle concentration beyond 1 mg/ml was obvious only for the largest particle size fractions SBA/90 and SBA/125.

Most MCM-41 samples tested at 4 mg/ml showed significantly higher $O_2^{\cdot-}$ formation in comparison with the corresponding SBA-15 samples (although at lower concentrations such difference was not evident). This result did not correlate with the higher caspase-3/7 activity of SBA-15 at 4 mg/ml (Fig. 6), or the cell viability data at 4 mg/ml (Figs. 3b and 5b), suggesting that the caspase-3/7 activity was also increased by other cytotoxic processes besides $O_2^{\cdot-}$ formation. Most probable reason was direct physical cell–particle interaction.

4. Discussion

The Caco-2 cells exist in a continuum of undifferentiated (or dividing), semi-differentiated and differentiated (or non-dividing) states of maturity. The undifferentiated Caco-2 cells were used in the present study, as the employed cytotoxicity assays were designed and optimized for these cells. The biochemical effects of

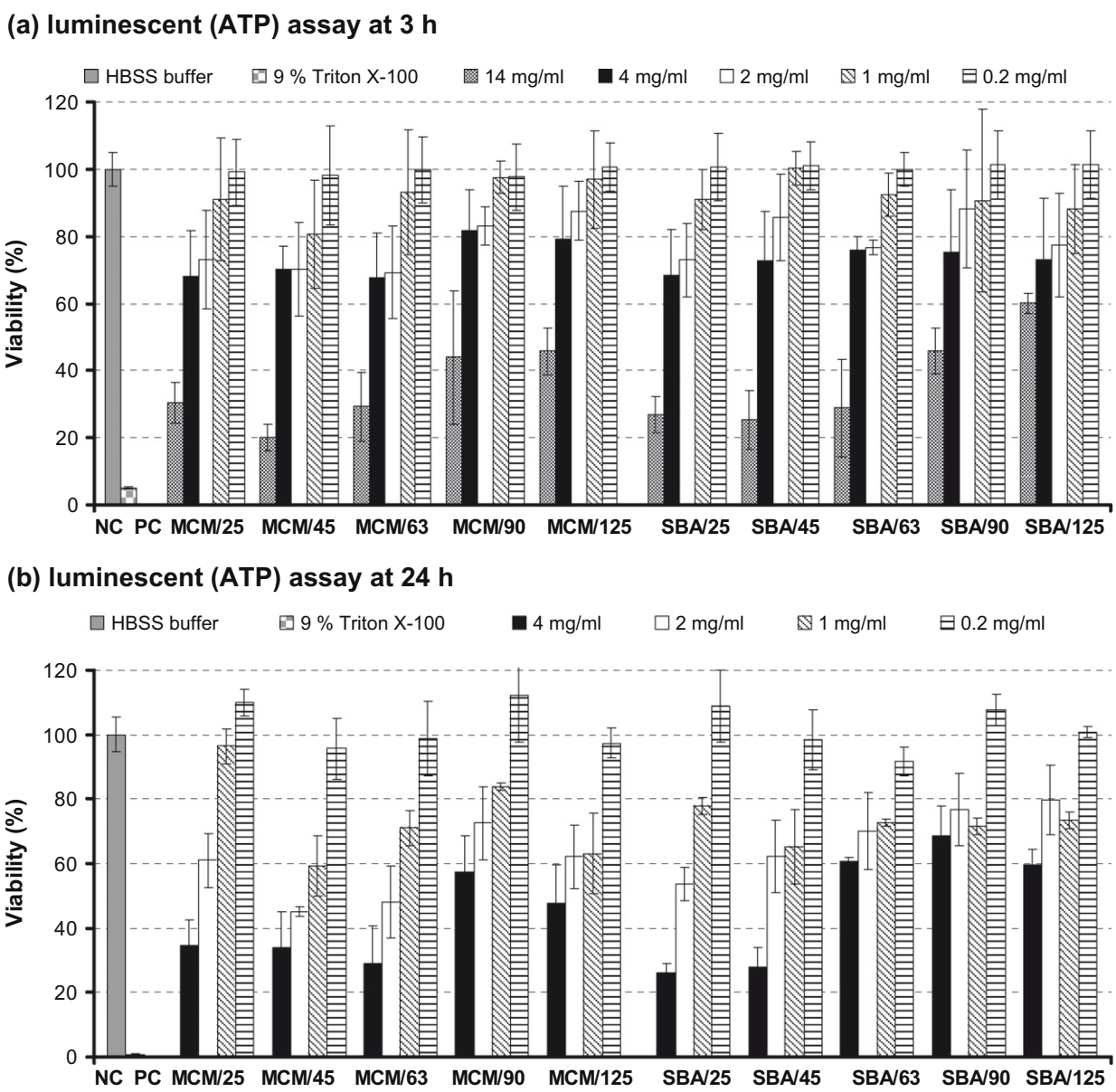

Fig. 5. Caco-2 cell viability results from luminescence assay after: (a) 3 h and (b) 24 h incubation with MCM-41 and SBA-15 samples at 37 °C, as a function of the particle concentration and size fraction ($n \geqslant 3 \pm$ SEM).

cyanotoxins on undifferentiated and differentiated Caco-2 cells after 24-h exposure have been reported similar considering the endpoints of cell protein content, neutral red uptake and metabolism [38]. Still, the undifferentiated Caco-2 cells are sensitive to direct external perturbation by the particles. Although this facilitated the monitoring of very slight deleterious cell–particle interactions, it was likely that the effect was exaggerated in comparison with differentiated Caco-2 cell monolayers or actual intestinal epithelium. The commonly used lactate dehydrogenase (LDH) cell membrane integrity assay was not used in the present study, as it was recently reported to interact with 15 nm silica nanoparticles and give a false positive signal on Caco-2 cells (however a luminescent ATP assay was reported to work correctly, showing significant ATP depletion for 15 nm silica nanoparticles after 4-h exposure to 1 mg/ml, while 200 nm fumed silica had no effect) [39].

The ordered mesoporous silica microparticles of MCM-41 and SBA-15 induced significant time- and mass dose-dependent effects on the Caco-2 cells considering the studied endpoints, while the effect of the tested particle size fraction or silica material was variable. The metabolic activity of the cells was the more sensitive endpoint over the cell membrane integrity assay towards detecting deleterious effects of the silica particulates. The metabolic activity of the cells significantly reduced already after 3-h exposure time at doses lower than the significant effect threshold in the fluorescence test. To illustrate, significant ATP depletion was observed for most samples already after 3-h incubation with 2–4 mg/ml of the particles, while no effect on the cell membrane integrity was detected under the same conditions (excluding the samples with high relative small microparticle content). Since the early ATP depletion was not directly associated with a large-scale physical cell membrane injury, the involvement of reactive oxygen species (ROS) as the root cause was studied. The deleterious effect of oxidative stress on the proper function of cells is well known, and also Caco-2 cells have been reported to be sensitive to ROS damage [40,41]. Standard silicas are known initiators of ROS generation, e.g. activation of caspase-3 has been linked to silica-induced

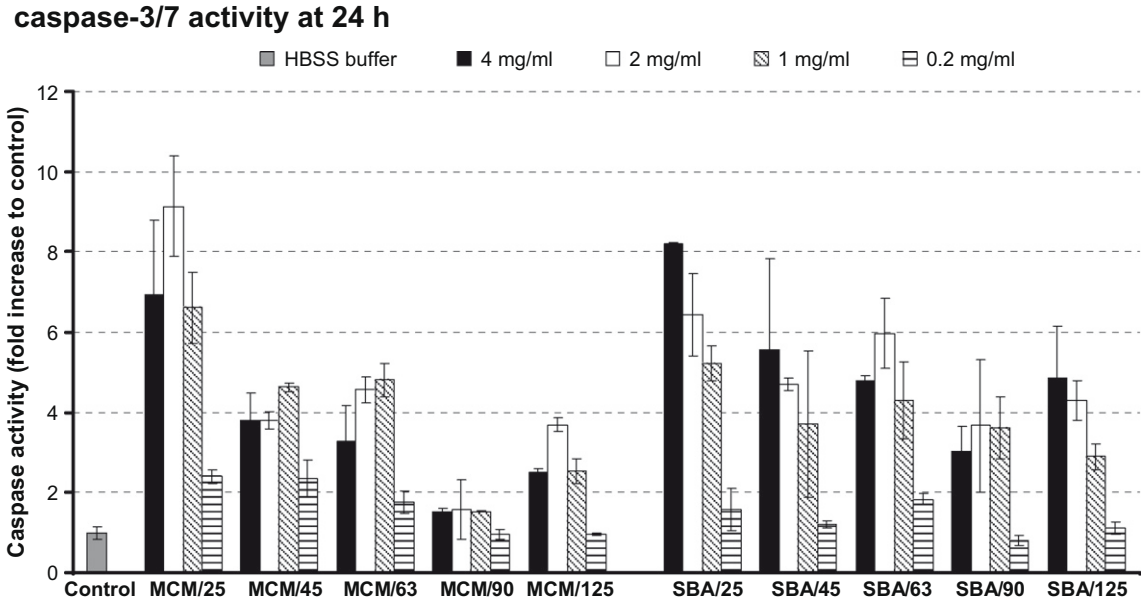

Fig. 6. Caspase-3/7 activity for the Caco-2 cells after being treated and incubated for 24 h with MCM-41 and SBA-15 samples at 37 °C, as a function of the particle concentration and size fraction ($n \geqslant 3 \pm$ SEM). Results are expressed as a ratio between treated and untreated cells.

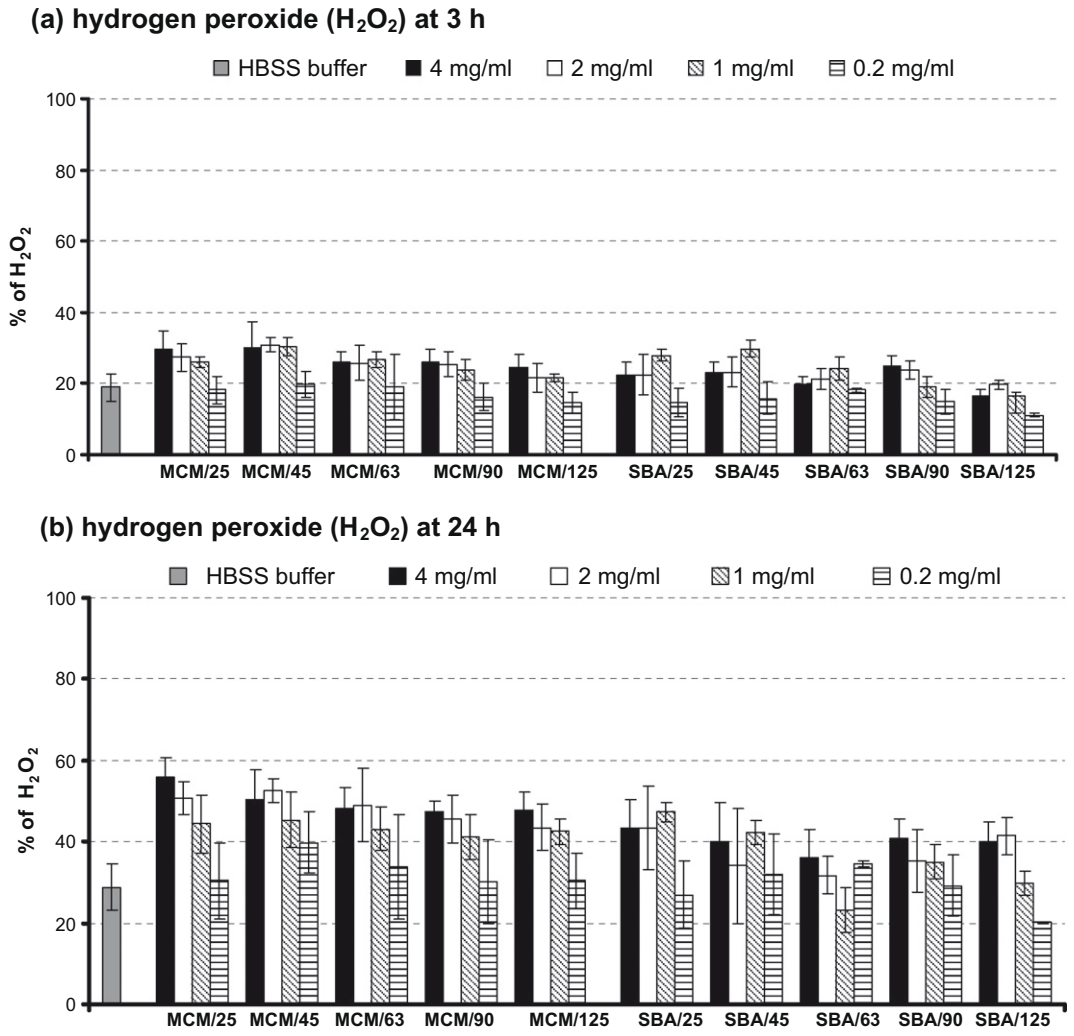

Fig. 7. Results of hydrogen peroxide (H_2O_2) detection by DCF-DA staining of the Caco-2 cells after being treated and incubated with MCM-41 and SBA-15 samples for: (a) 3 h and (b) 24 h at 37 °C, as a function of the particle concentration and size fraction ($n = 4 \pm$ SEM). Results are expressed as a percentage of the control.

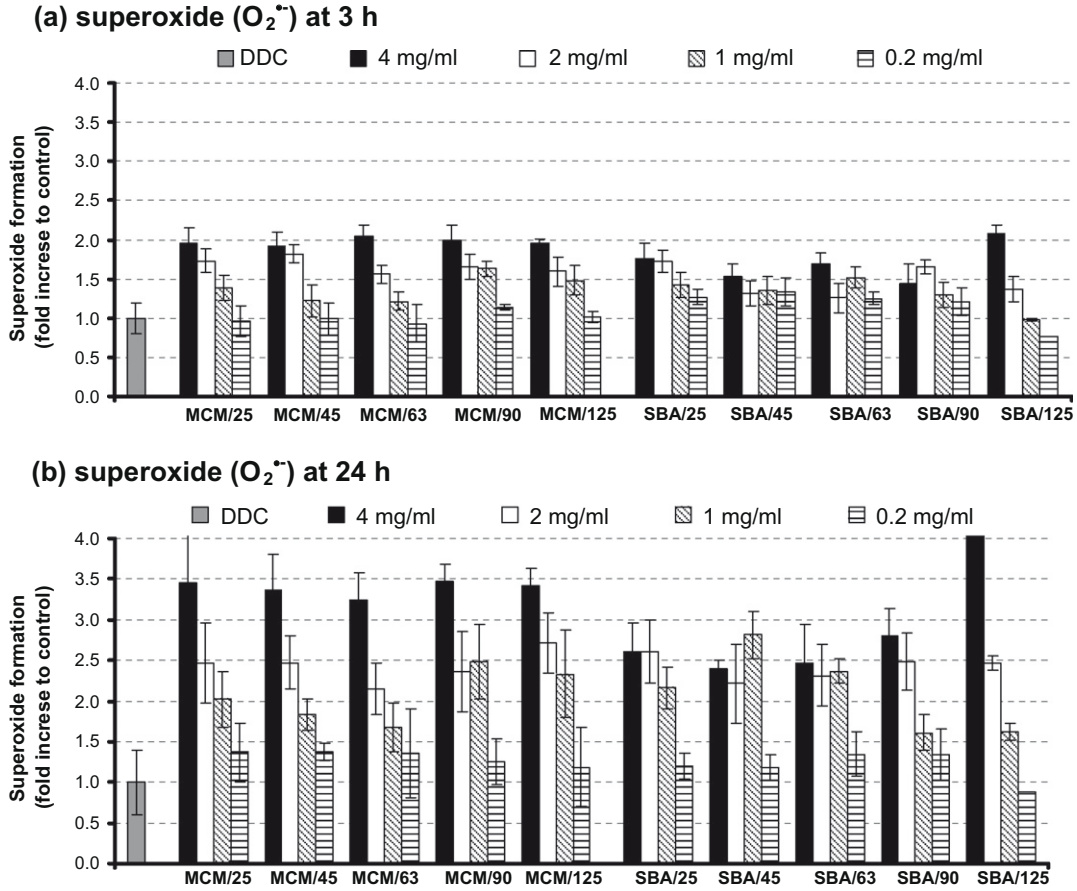

Fig. 8. Results of superoxide ($O_2^{\bullet-}$) detection by DHE staining of the Caco-2 cells after being treated and incubated with MCM-41 and SBA-15 samples for: (a) 3 h and (b) 24 h at 37 °C, as a function of the particle concentration and size fraction ($n = 4 \pm$ SEM). Results are expressed as a ratio between the treated and untreated cells.

formation of ROS [11,18]. Our results demonstrated for the first time that also ordered mesoporous silica MCM-41 and SBA-15 initiate the formation of ROS with Caco-2 cells, especially the superoxide $O_2^{\bullet-}$ radical, already after 3-h exposure to a dose of 1 mg/ml. The superoxide radical is known as the precursor for most other oxidative species, including H_2O_2, and as the most proximal ROS considering the mitochondrial function, e.g. ATP synthesis [42,43]. The results of the present study evidenced that the initial mechanism of cytotoxicity of the MCM-41 and SBA-15 particulates was the increase in $O_2^{\bullet-}$ formation that was translated to ATP depletion. However, the initial ATP depletion did not affect the Caco-2 cell membrane integrity, which was in accordance with the results of a previous report of ATP and LDH assay on Caco-2 cells showing that elevated levels of $O_2^{\bullet-}$ are not directly responsible for cell membrane damage [44]. H_2O_2 species can react with the silica surface radicals $SiO^{\bullet}$, $SiO_2^{\bullet}$, $SiO_3^{\bullet}$, $Si^{+}O_2^{\bullet-}$ forming the $HO^{\bullet}$ radical, which has been suggested to be involved in cell membrane damage via lipid peroxidation [19,43]. The substantiated cell membrane damage detected at 3 h for samples MCM/25 and MCM/45 was likely partly due to the heightened levels of H_2O_2, although direct physical interaction with the particles was the more important process as the decrease in AFC viability data was so drastic in comparison with the other samples. The caspase-3/7 activity of all samples at 24 h increased significantly (~2–10-fold increase to control) when the tested particle concentration was 1 mg/ml, while also significant ATP depletion was detected. Heightened ROS level has been previously found to cause ATP depletion in Caco-2 cells (via the same luminescence assay as employed herein), as well as affect cell cycle progression by initiating apoptosis [45]. Also in the present study, the outcome of the initial $O_2^{\bullet-}$ formation at 3 h was drastically increased apoptotic signalling activity in the cells at 24 h, indicating an overwhelming of the cells antioxidant defences.

Besides the formation of ROS, it was evident in the results that also direct cell–particle interactions were involved in the overall mechanism of cytotoxicity. Samples MCM/25 and MCM/45 had a higher relative volume content of small particles (<5 μm) in comparison with the other samples, which may be the reason for their substantiated results. Previously, small microparticles (2.5 ± 0.5 μm) of AMS-8 type mesoporous silica have been found to actively internalize cells (MDDC) during 1-h exposure, translating to significantly increased amount of apoptotic/necrotic MDDC after 24 h [46]. Also, Caco-2 cells have been reported to internalize (co-polymer) particles of size 0.1 μm and 1 μm in significantly higher mass or number in comparison with 10 μm particles after 2 h [47]. Caco-2 internalization of the smallest MCM-41 and SBA-15 microparticles and their direct effects on the cell membrane remain to be evaluated in the future by cellular uptake and confocal microscopy studies. Since the mesopores in the MCM-41 and SBA-15 particles are very small in diameter in comparison with the size of the Caco-2 cells, only the external surface area of the particles can directly interact with the cell membrane. However, no satisfactory correlation was found for the AFC and ATP cell viability data and the properties of the particles, such as external surface and BET area (Table 1). Indeed, the mesoporous property of silicas has not been found to significantly affect their cytotoxicity in previous studies [48]. However, whether the large BET surface area of MCM-41 and SBA-15 materials induces higher ROS formation in comparison with non-porous bulk silicas should be determined in the future. One might assume that the acicular (or needle-like) particles of sample SBA/125 (and SBA/90 to some extent) would puncture the cell membranes more easily

compared to particles of more rounded shape. However, the assay results for SBA/125 did not systematically support such effect. Although moderate cell membrane damage was detected for SBA/125 in the 24 h AFC assay at concentration of 1–2 mg/ml (Fig. 3b) in comparison with the other samples, the result at 4 mg/ml did not follow this trend. As the other assays also did not support the deviant behaviour of SBA/125 at 1–2 mg/ml, it was concluded that the acicular shape of large (~100 μm) particles was not important considering the overall cytotoxic effect. Still, the cytotoxic effect of small (<5 μm) acicular particles and similar size rounded particles should be compared in future studies, also taking into account their total number in the dose.

5. Conclusions

We have investigated the cytotoxic effects of ordered mesoporous silica MCM-41 and SBA-15 microparticles on the human colon carcinoma Caco-2 cells for the first time. The results evidenced that MCM-41 and SBA-15 microparticles caused cytotoxic effects on the Caco-2 cells, at most tested concentrations and incubation times. The effects on the cells included weakened cell membrane integrity, diminished cell metabolism and increased apoptotic signalling. Particles tested at the threshold concentration of 2 mg/ml were found to induce significant ATP depletion in the cells already after 3 h, which was the most sensitive cellular endpoint in the study. The root cause for the deleterious effects of the particles was the heightened production of reactive oxygen species (ROS), especially the formation of the superoxide radical $O_2^{\cdot-}$ after 3 h at concentration 1 mg/ml, apparently overwhelming the antioxidant defences and causing mitochondrial dysfunction, hence increasing the apoptotic signalling (caspase-3/7 activity). The $O_2^{\cdot-}$ formation increased when the particle concentration and incubation time was increased. Interaction of small microparticles (⩽5 μm) with the cells was another major route of cytotoxicity, apparently by inflicting direct physical damage (puncture) on the cell membrane and/or causing apoptotic signalling after cellular uptake.

Comparing in vitro results to in vivo situation is notoriously difficult, especially in the case of a complex and fluctuating physiological system as the GIT. In vivo, the contact time of the particles with the epithelial cells of the intestine would continuously change as the particles move along the GIT (typical transit time 199 ± 78 min [49]). It is also possible that some of the particles would be trapped in sites as between the villi or in the crypts, increasing the local concentration of the particles for extended periods (most fluid circulating in the GIT is absorbed in the small intestine, leaving some 54–105 ml of fluid at separated pockets [50]). The selected test parameters (concentration/time) used herein should cover a wide range of conditions of cell–particle interaction that might actually take place in vivo. Still, for example the side-effects of intestinal epithelial cell uptake and potential mucosal passage of small microparticles, as well as nanoparticles, from the intestinal lumen to the vascular compartment should be considered in future studies. Based on the present results, it would be especially important to carefully control the microparticle size of MCM-41 and SBA-15 used in an oral formulation, avoiding the use of the smallest microparticles.

Acknowledgements

The financial support from the Academy of Finland (Grants Nos. 122314, 123037, 118002 and 127099), Finnish Academy of Science and Letters, Turku University Foundation, Otto Malm Foundation and the University of Helsinki Research Funds is acknowledged. Prof. T. Salmi (Laboratory of Industrial Chemistry, Åbo Akademi University) is acknowledged for scientific collaboration. MSc L. Uotila (Department of Biological and Environmental Sciences, University of Helsinki) is acknowledged for technical assistance with the flow cytometer method. MSc J. Riikonen and MSc E. Mäkilä are acknowledged for technical assistance with the laser diffraction method and LPh M. Heinonen for technical assistance with the SEM imaging (Department of Physics, University of Turku).

References

[1] J.S. Beck, J.C. Vartuli, W.J. Roth, M.E. Leonowicz, C.T. Kresge, K.D. Schmitt, C.T.W. Chu, D.H. Olson, E.W. Sheppard, S.B. McCullen, J.B. Higgins, J.L. Schlenker, A new family of mesoporous molecular-sieves prepared with liquid-crystal templates, J. Am. Chem. Soc. 114 (1992) 10834–10843.
[2] C.T. Kresge, M.E. Leonowicz, W.J. Roth, J.C. Vartuli, J.S. Beck, Ordered mesoporous molecular-sieves synthesized by a liquid-crystal template mechanism, Nature 359 (1992) 710–712.
[3] D.Y. Zhao, Q.S. Huo, J.L. Feng, B.F. Chmelka, G.D. Stucky, Nonionic triblock and star diblock copolymer and oligomeric surfactant syntheses of highly ordered, hydrothermally stable, mesoporous silica structures, J. Am. Chem. Soc. 120 (1998) 6024–6036.
[4] D.Y. Zhao, J.L. Feng, Q.S. Huo, N. Melosh, G.H. Fredrickson, B.F. Chmelka, G.D. Stucky, Triblock copolymer syntheses of mesoporous silica with periodic 50 to 300 angstrom pores, Science 279 (1998) 548–552.
[5] P. Horcajada, A. Ramila, J. Perez-Pariente, M. Vallet-Regi, Influence of pore size of MCM-41 matrices on drug delivery rate, Micropor. Mesopor. Mater. 68 (2004) 105–109.
[6] C.D. Nunes, P.D. Vaz, A.C. Fernandes, P. Ferreira, C.C. Romao, M.J. Calhorda, Loading and delivery of sertraline using inorganic micro and mesoporous materials, Eur. J. Pharm. Biopharm. 66 (2007) 357–365.
[7] M. Vallet-Regi, A. Ramila, R.P. del Real, J. Perez-Pariente, A new property of MCM-41: drug delivery system, Chem. Mater. 13 (2001) 308–311.
[8] Y.J. Han, G.D. Stucky, A. Butler, Mesoporous silicate sequestration and release of proteins, J. Am. Chem. Soc. 121 (1999) 9897–9898.
[9] S.W. Song, K. Hidajat, S. Kawi, Functionalized SBA-15 materials as carriers for controlled drug delivery: influence of surface properties on matrix–drug interactions, Langmuir 21 (2005) 9568–9575.
[10] M. Vallet-Regi, Ordered mesoporous materials in the context of drug delivery systems and bone tissue engineering, Chem. Eur. J. 12 (2006) 5934–5943.
[11] B. Fubini, A. Hubbard, Reactive oxygen species (ROS) and reactive nitrogen species (RNS) generation by silica in inflammation and fibrosis, Free Radic. Bio. Med. 34 (2003) 1507–1516.
[12] D. Warshawsky, R. Reilman, J. Cheu, M. Radike, C. Rice, Influence of particle dose on the cytotoxicity of hamster and rat pulmonary alveolar macrophage in-vitro, J. Toxicol. Environ. Health A 42 (1994) 407–421.
[13] B.Z. Zhong, W.Z. Whong, T.M. Ong, Detection of mineral-dust-induced DNA damage in two mammalian cell lines using the alkaline single cell gel/comet assay, Mutat. Res-Genet. Toxicol. Environ. 393 (1997) 181–187.
[14] S.C. Brown, M. Kamal, N. Nasreen, A. Baumuratov, P. Sharma, V.B. Antony, B.M. Moudgil, Influence of shape, adhesion and simulated lung mechanics on amorphous silica nanoparticle toxicity, Adv. Powder Technol. 18 (2007) 69–79.
[15] L. Mollo, V. Levresse, M.F. Ottaviani, S. ElloukAchard, M.C. Jaurand, B. Fubini, Study of the stability of a paramagnetic label linked to mesoporous silica surface in contact with rat mesothelial cells in culture, Environ. Health Persp. 105 (1997) 1031–1036.
[16] K.M. Waters, L.M. Masiello, R.C. Zangar, N.J. Karin, R.D. Quesenberry, S. Bandyopadhyay, J.G. Teeguarden, J.G. Pounds, B.D. Thrall, Macrophage responses to silica nanoparticles are highly conserved across particle sizes, Toxicol. Sci. 107 (2009) 553–569.
[17] A. Nel, T. Xia, L. Madler, N. Li, Toxic potential of materials at the nanolevel, Science 311 (2006) 622–627.
[18] R.F. Hamilton, S.A. Thakur, A. Holian, Silica binding and toxicity in alveolar macrophages, Free Radic. Bio. Med. 44 (2008) 1246–1258.
[19] Z. Elias, O. Poirot, M.C. Daniere, F. Terzetti, A.M. Marande, S. Dzwigaj, H. Pezerat, I. Fenoglio, B. Fubini, Fg, Cytotoxic and transforming effects of silica particles with different surface properties in Syrian hamster embryo (SHE) cells, Toxicol. in Vitro 14 (2000) 409–422.
[20] Z. Elias, O. Poirot, I. Fenoglio, M. Ghiazza, M.C. Daniere, F. Terzetti, C. Darne, C. Coulais, I. Matekovits, B. Fubini, Surface reactivity, cytotoxic, and morphological transforming effects of diatomaceous earth products in Syrian hamster embryo cells, Toxicol. Sci. 91 (2006) 510–520.
[21] D.M. Huang, Y. Hung, B.S. Ko, S.C. Hsu, W.H. Chen, C.L. Chien, C.P. Tsai, C.T. Kuo, J.C. Kang, C.S. Yang, C.Y. Mou, Y.C. Chen, Highly efficient cellular labeling of mesoporous nanoparticles in human mesenchymal stem cells: implication for stem cell tracking, FASEB 19 (2005) 2014–2016.
[22] T.H. Chung, S.H. Wu, M. Yao, C.W. Lu, Y.S. Lin, Y. Hung, C.Y. Mou, Y.C. Chen, D.M. Huang, The effect of surface charge on the uptake and biological function of mesoporous silica nanoparticles 3T3-L1 cells and human mesenchymal stem cells, Biomaterials 28 (2007) 2959–2966.
[23] C.Y. Lai, B.G. Trewyn, D.M. Jeftinija, K. Jeftinija, S. Xu, S. Jeftinija, V.S.Y. Lin, A mesoporous silica nanosphere-based carrier system with chemically removable CdS nanoparticle caps for stimuli-responsive controlled release of neurotransmitters and drug molecules, J. Am. Chem. Soc. 125 (2003) 4451–4459.
[24] J. Lu, M. Liong, J.I. Zink, F. Tamanoi, Mesoporous silica nanoparticles as a delivery system for hydrophobic anticancer drugs, Small 3 (2007) 1341–1346.

[25] I. Slowing, B.G. Trewyn, V.S.Y. Lin, Effect of surface functionalization of MCM-41-type mesoporous silica nanoparticles on the endocytosis by human cancer cells, J. Am. Chem. Soc. 128 (2006) 14792–14793.
[26] Y.S. Lin, C.P. Tsai, H.Y. Huang, C.T. Kuo, Y. Hung, D.M. Huang, Y.C. Chen, C.Y. Mou, Well-ordered mesoporous silica nanoparticles as cell markers, Chem. Mater. 17 (2005) 4570–4573.
[27] S.P. Hudson, R.F. Padera, R. Langer, D.S. Kohane, The biocompatibility of mesoporous silicates, Biomaterials 29 (2008) 4045–4055.
[28] T. Heikkila, J. Salonen, J. Tuura, N. Kumar, T. Salmi, D.Y. Murzin, M.S. Hamdy, G. Mul, L. Laitinen, A.M. Kaukonen, J. Hirvonen, V.P. Lehto, Evaluation of mesoporous TCPSi, MCM-41, SBA-15 and TUD-1 materials as API carriers for oral drug delivery, Drug Deliv. 14 (2007) 337–347.
[29] T. Heikkila, J. Salonen, J. Tuura, M.S. Hamdy, G. Mul, N. Kumar, T. Salmi, D.Y. Murzin, L. Laitinen, A.M. Kaukonen, J. Hirvonen, V.P. Lehto, Mesoporous silica material TUD-1 as a drug delivery system, Int. J. Pharm. 331 (2007) 133–138.
[30] R. Mellaerts, C.A. Aerts, J. Van Humbeeck, P. Augustijns, G. Van den Mooter, J.A. Martens, Enhanced release of itraconazole from ordered mesoporous SBA-15 silica materials, Chem. Commun. 13 (2007) 1375–1377.
[31] C. Charnay, S. Begu, C. Tourne-Peteilh, L. Nicole, D.A. Lerner, J.M. Devoisselle, Inclusion of ibuprofen in mesoporous templated silica: drug loading and release property, Eur. J. Pharm. Biopharm. 57 (2004) 533–540.
[32] V. Ambrogi, L. Perioli, F. Marmottini, S. Giovagnoli, M. Esposito, C. Rossi, Improvement of dissolution rate of piroxicam by inclusion into MCM-41 mesoporous silicate, Eur. J. Pharm. Sci. 32 (2007) 216–222.
[33] R. Mellaerts, R. Mols, J.A.G. Jammaer, C.A. Aerts, P. Annaert, J. Van Humbeeck, G. Van den Mooter, P. Augustijns, J.A. Martens, Increasing the oral bioavailability of the poorly water soluble drug itraconazole with ordered mesoporous silica, Eur. J. Pharm. Biopharm. 69 (2008) 223–230.
[34] A.J. Pasqua, K.K. Sharma, Y.-L. Shi, B.T. Bonnie, W. Oullette, J.C. Dabrowiak, T. Asefa, Cytotoxicity of mesoporous silica nanoparticles, J. Inorg. Biochem. 102 (2008) 1416–1423.
[35] A. Bernas, P. Laukkanen, N. Kumar, P. Maki-Arvela, J. Vayrynen, E. Laine, B. Holmbom, T. Salmi, D.Y. Murzin, A new heterogeneously catalytic pathway for isomerization of linoleic acid over Ru/C and Ni/H–MCM-41 catalysts, J. Catal. 210 (2002) 354–366.
[36] W.M. Hua, Y.H. Yue, Z. Gao, Acidity enhancement of SBA mesoporous molecular sieve by modification with SO_4^{2-}/ZrO_2, J. Mol. Catal. A-Chem. 170 (2001) 195–202.
[37] A.P. Tinke, A. Carnicer, R. Govoreanu, G. Scheltjens, L. Lauwerysen, N. Mertens, K. Vanhoutte, M.E. Brewster, Particle shape and orientation in laser diffraction and static image analysis size distribution analysis of micrometer sized rectangular particles, Powder Technol. 186 (2008) 154–167.
[38] M. Puerto, S. Pichardo, A. Jos, A.M. Camean, Comparison of the toxicity induced by microcystin-RR and microcystin-YR in differentiated and undifferentiated Caco-2 cells, Toxicon 54 (2009) 161–169.
[39] B. Wahl, N. Daum, H.-L. Ohrem, C.-M. Lehr, Novel luminescence assay offers new possibilities for the risk assessment of silica nanoparticles, Nanotoxicology 4 (2008) 243–251.
[40] T. Noda, R. Iwakiri, K. Fujimoto, T.Y. Aw, Induction of mild intracellular redox imbalance inhibits proliferation of Caco-2 cells, FASEB J. 15 (2001) 2131–2139.
[41] B. Zegura, M. Volcic, T.T. Lah, M. Filipic, Different sensitivities of human colon adenocarcinoma (Caco-2), astrocytoma (IPDDC-A2) and lymphoblastoid (NCNC) cell lines to microcystin-LR induced reactive oxygen species and DNA damage, Toxicon 52 (2008) 518–525.
[42] M.P. Murphy, How mitochondria produce reactive oxygen species, Biochem. J. 417 (2009) 1–13.
[43] J.F. Turrens, Mitochondrial formation of reactive oxygen species, J. Physiol.-London 552 (2003) 335–344.
[44] B.R. Gebhardt, J. Ries, W.F. Caspary, H. Boehles, J. Stein, Superoxide: a major factor for stress protein induction in reoxygenation injury in the intestinal cell line Caco-2, Digestion 60 (1999) 238–245.
[45] I. Elisia, D.D. Kitts, Anthocyanins inhibit peroxyl radical-induced apoptosis in Caco-2 cells, Mol. Cell. Biochem. 312 (2008) 139–145.
[46] H. Vallhov, S. Gabrielsson, M. Stromme, A. Scheynius, A.E. Garcia-Bennett, Mesoporous silica particles induce size dependent effects on human dendritic cells, Nano Lett. 7 (2007) 3576–3582.
[47] M.P. Desai, V. Labhasetwar, E. Walter, R.J. Levy, G.L. Amidon, The mechanism of uptake of biodegradable microparticles in Caco-2 cells is size dependent, Pharm. Res. 14 (1997) 1568–1573.
[48] I. Fenoglio, A. Croce, F. Di Renzo, R. Tiozzo, B. Fubini, Pure-silica zeolites (porosils) as model solids for the evaluation of the physicochemical features determining silica toxicity to macrophages, Chem. Res. Toxicol. 13 (2000) 489–500.
[49] L.X. Yu, J.R. Crison, G.L. Amidon, Compartmental transit and dispersion model analysis of small intestinal transit flow in humans, Int. J. Pharm. 140 (1996) 111–118.
[50] C. Schiller, C.P. Frohlich, T. Giessmann, W. Siegmund, H. Monnikes, N. Hosten, W. Weitschies, Intestinal fluid volumes and transit of dosage forms as assessed by magnetic resonance imaging, Aliment. Pharmcol. Ther. 22 (2005) 971–979.